Field Emission Property of Carbon Nanotube Field Emitters in Triode Structure Fabricated with Anodic Aluminum Oxide Templates

2008 Jpn. J. Appl. Phys. 47 3282

(http://iopscience.iop.org/1347-4065/47/4S/3282)

Japanese Journal of Applied Physics
Vol. 47, No. 4, 2008, pp. 3282–3286

Field Emission Property of Carbon Nanotube Field Emitters in Triode Structure Fabricated with Anodic Aluminum Oxide Templates

Yiming LI*, Hui-Wen CHENG, Chen-Chun LIN[1], and Fu-Ming PAN[1]

Department of Communication Engineering, National Chiao Tung University, 1001 Ta-Hsueh Road, Hsinchu 300, Taiwan
[1]*Department of Materials Science and Engineering, National Chiao Tung University, 1001 Ta-Hsueh Road, Hsinchu 300, Taiwan*

(Received October 2, 2007; accepted December 11, 2007; published online April 25, 2008)

In this work, we study the field emission (FE) properties of carbon nanotubes (CNTs) field emitters in the triode structure fabricated with anodic aluminum oxide (AAO) template. To obtain the self-consistent solution, a set of Maxwell's equations coupling with Lorentz equation are solved simultaneously using finite difference time domain (FDTD) particle-in-cell (PIC) method. The FE current is then computed with the Fowler–Nordheim equation. To validate our simulation model, we firstly calibrate the collected electron current density between the measurement data of fabricated AAO–CNTs and simulation result. We find that the high density of CNTs will result in large screening effect among adjacent emitters and reduce the strength of electric field. Consequently, it significantly affects the collected emission current density. Our prediction shows that more than three-order magnitude difference on the collected emission current density could be observed when the spacing between CNTs is decreased from 0.7 to 0.233 μm for the explored structure with the diameter of 7 μm. Effects of random heights and thickness of oxide on the FE property of structure are also discussed. [DOI: 10.1143/JJAP.47.3282]

KEYWORDS: carbon nanotubes, anodic aluminum oxide, triode structure, field emission, Maxwell's equation, Lorentz equation, numerical simulation, FDTD-PIC method, Fowler–Nordheim equation

1. Introduction

Carbon nanotubes (CNTs) are promising in cold-cathode flat panel displays for their chemical stability, mechanical strength, and electron emission properties.[1,2] A triode-typed field emission display possesses stable and effective emissions and high quality screen which is superior to a diode-typed one. To pursue uniform and high emission current density, it is necessary to grow vertically aligned CNT arrays on a large area with suitable tube density and tube diameters. Various template-fabrication methods have been reported;[3,4] in particular, anodic aluminum oxide (AAO) nanotemplates because AAO has vertical pore channels, highly ordered pore arrangement, and uniform pore size. Study on uniformity of the filed emission (FE) property of AAO–CNTs benefits the growth of novel structures.

In this work, new FE triode arrays with the AAO template CNTs as the field emitters are successfully fabricated and analyzed. Fabrication of AAO–CNTs is using standard integrated circuit processes in our recent work.[5] A finite-difference time domain particle-in-cell numerical simulation[6–9] is adopted to examine the FE property in the CNT FE triode structure with the AAO template. According to our calibration, simulated data shows good agreement with the measured emission current of the AAO–CNT in the triode structure. We thus explore the effect of density and morphology of the CNTs on the uniformity of FE properties of AAO–CNT in the triode structure. We find that the high density of CNTs will result in large screening effect among adjacent emitters and reduce the strength of electric field. Consequently, it significantly affects the collected emission current density that has more than three-order magnitude variation. Considering the manufacturability of growth, optimal conditions on the number and height of CNTs are examined accordingly.

This paper is organized as follows. In §2, we state the fabricated AAO–CNTs triode structure and simulation model. In §3, we show the results and discussion. Finally, we draw conclusions and suggestion future work.

2. Fabricated Sample and Simulation Model

Figure 1 shows scanning electron microscopy (SEM) images of the fabricated samples. The AAO–CNTs triodes are with a diameter of 7 μm, the tetraethoxysilane oxide 1 μm is the dielectric layer of the triode, and a 0.5-μm-thick Al layer is the gate electrode. A 2-μm-thick Al film is deposited on the Si wafer, and the AAO pore channel array is subsequently prepared by electrochemical anodization in 0.3 M oxalic acid solution at 21 °C under a constant polarization voltage of 40 V for 5 min. The thus formed nanoporous AAO about 1 μm thick was removed by wet chemical etching at 60 °C with a mixture solution of H_3PO_4 and CrO_3, thereby leaving a relatively ordered indent pattern on the surface of the Al film. The second anodization of the indented Al film was then performed for 4 min under the same anodization condition as the first one. After the second anodization step, the AAO barrier layer removal and pore widening were performed by etching the as-prepared AAO film in a 5 wt % H_3PO_4 solution at 30 °C for 40 min. This resulted in highly uniform and periodic nanoporous channels in the AAO layer, which were then used as the template for the growth of carbon nanotubes. A metallic Al layer $\approx$ 300 nm thick was left on the wafer surface after the AAO fabrication, and was used as the bottom electrode. Cobalt was used as the catalyst for CNT growth, and was electrochemically deposited at the AAO pore bottom in the mixture electrolyte of $CoSO_4$ and H_3BO_3. The length and tube density of CNTs extending out of the AAO pore channels could be properly controlled by the growth time and the gas ratio of CH_4 and H_2 in the electron cyclotron resonance chemical vapor deposition (ECR-CVD) system, respectively. The CNT emitters are grown in an ECR-CVD system at 600 °C, and the CNTs grow along the axis of pore channels and have a tube diameter compliant with the pore size of the AAO pore channels, resulting in uniform diameter and well-aligned emitters. AAO pore channel array has highly ordered

*E-mail address: ymli@faculty.nctu.edu.tw

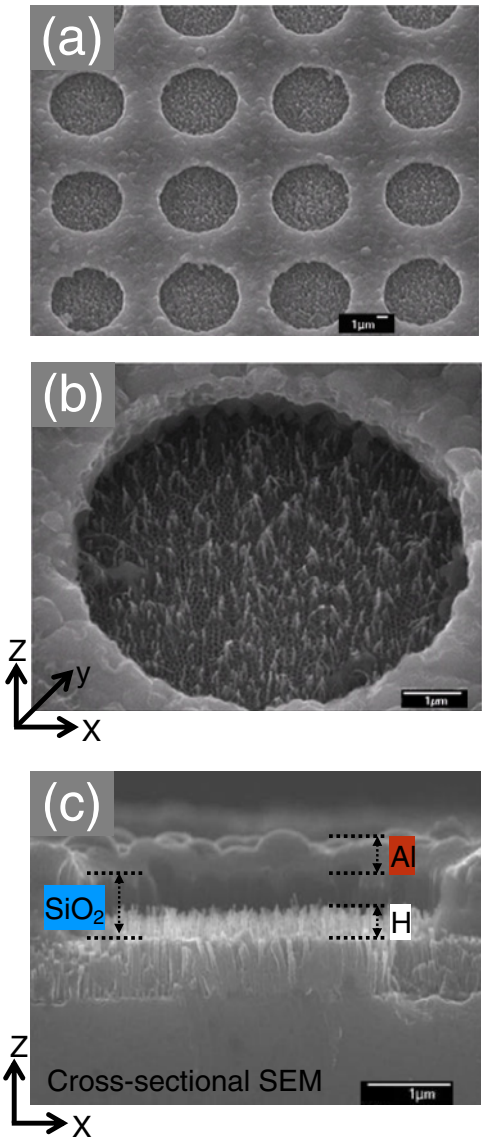

Fig. 1. (Color online) (a) The SEM image of the fabricated AAO–CNTs triode array. (b) An enlarged plot of (a) for a single triode. The scalar bars are equal to 1 μm for both images. (c) The cross-sectional view of (b).

pore arrangement with a uniform pore size of 70–80 nm and the length of the vertical pore channel is about 700 nm. With a symmetrical property of the fabricated AAO–CNTs along the growth direction, as shown in Fig. 1(c), the FE property of the fabricated sample is calculated numerically.

A schematic plot of the two-dimensional (2D) simulation domain of the structure in shown in Fig. 2. The setting of the 2D simulation domain is mainly according to the cylindrical symmetry of the structure of AAO–CNTs, as shown in the inset of Fig. 2. Finite-difference time domain particle-in-cell (FDTD-PIC) numerical simulation method[6–9] is implemented to investigate emission current of the AAO–CNTs for the region form by ABCD, as shown in Fig. 2. To explore the electron-emission properties in the explored structure, the electromagnetic particle-in-cell (PIC) scheme[6–9] is used; starting from a specified initial state, we evaluate the electrostatic field along the emitter surface which is determined for a given geometry and applied voltage. In the field emission process, the electron emission is modeled by the Fowler–Nordheim (F–N) equation[10]

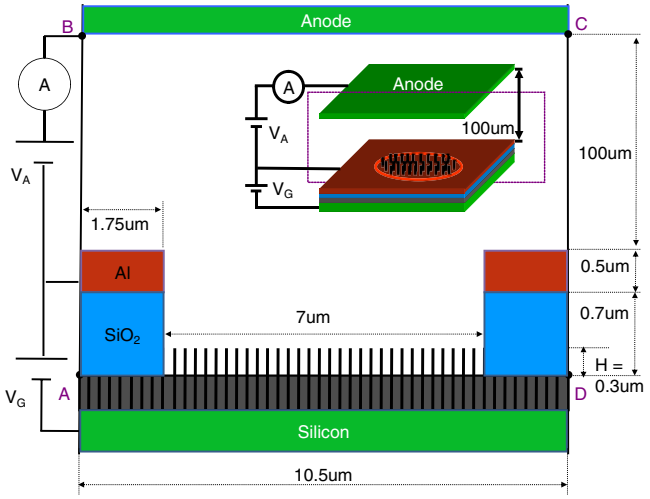

Fig. 2. (Color online) Along the dotted line, the cross-sectional plot of the inset figure shows the 2D simulation domain of AAO–CNTs triode.

$$J = \frac{AE^2}{\varphi t^2}\exp\left(\frac{-Bv(y)\varphi^{3/2}}{E}\right), \tag{1}$$

where $A = 1.541 \times 10^{-6}\,\mathrm{A\,eV/V^2}$, E is the normal component of the electric field at the emitter surface, φ is the work function of the emission material, t^2 is approximately equal to 1.1, and $v(y) = 0.95 - y^2$ with $y = 3.79 \times 10^{-5} \times E^{1/2}/\varphi$ is in SI unit. The fitting parameter B in eq. (1) reflects the slope[10,12–14] of the current density which depends upon the strength of electric field and should be calibrated with the experimentally collected current density. The emission current density is determined by eq. (1) according to the local electric field, the work function of emitter material, and the fitting parameters. The weighted charge density and current density at the grids are subsequently calculated. The obtained charge density and current density are successively used as sources in the Maxwell equations for advancing the electromagnetic fields. We then perform a time integration of Faraday's law, Ampere's law, and the relativistic Lorentz equation,[9]

$$\begin{aligned}
\frac{\partial \mathbf{B}}{\partial t} &= -\nabla \times \mathbf{E}, \\
\frac{\partial \mathbf{E}}{\partial t} &= -\frac{\mathbf{J}}{\varepsilon} + \frac{1}{\mu\varepsilon}\nabla \times \mathbf{B}, \\
\mathbf{F} &= q(\mathbf{E} + \mathbf{v} \times \mathbf{B}), \\
\frac{\partial \mathbf{x}}{\partial t} &= \mathbf{v},
\end{aligned} \tag{2}$$

subject to constraints provided by Gauss's law and the rule of divergence of $\mathbf{B}$,

$$\nabla \cdot \mathbf{E} = \frac{\rho}{\varepsilon} \quad \text{and} \quad \nabla \cdot \mathbf{B} = 0. \tag{3}$$

We notice that $\mathbf{E}$ and $\mathbf{B}$ are the electric and magnetic fields, $\mathbf{x}$ is the position of charge particle, and $\mathbf{J}$ and ρ are the current density and charge density resulting from charge particles. The full set of Maxwell's time-dependent equations is numerically solved to obtain electromagnetic fields. Similarly, the Lorentz force equation is solved to obtain relativistic particle trajectories. The charged particles are moved according to the Lorentz equation using the fields

advanced in each time step. These steps are repeated for each time step until the specified number of time steps is reached. We notice that the space-charge effects[11] are automatically included in the solution procedure. This 2D FDTD-PIC thus approaches to self-consistent simulation of the electromagnetic fields and charged particles.

3. Results and Discussion

We notice that due to the cylindrical symmetry of the fabricated structure, as shown in Fig. 1(b), the simulation domain can be simplified into a 2D one, as shown in Fig. 2(b). The results thus can be converted into 3D domain by multiplying the area of the structure. Calibration between the measured (the solid line) and simulated (the dash line) collected electron-emission current density versus the applied voltage (V_A) is first performed, as shown in Fig. 3, where all settings of parameters are the same with the indicated values of Fig. 2(b). We notice that the FDTD-PIC simulation belongs to time-domain calculation, so we calibrate data every 5 V for V_A ranging from 0 to 1000 V. According to this simulation technique, the computed result shows good agreement with the measurement, and the accuracy of this calculation could be justified through the measurement and 2D simulation of the fabricated sample. As shown in the inset of Fig. 3, the parameter B increases when V_A increases. It also implies, from eq. (1), that the corresponding F–N plot [i.e., a plot of $\ln(I/V^2)$ versus $1/V$] of the field emission of AAO–CNTs could be computed accordingly. Using the calibrated results, we now explore FE property due to the density and morphology of the CNT deposit. The FE property of the structure with single CNT is first shown in Fig. 4. The property is sensitively affected when the number of CNTs is increased due to the screening effect. The FE property is further suppressed when the number of CNTs is increased to 30, as shown in Fig. 6. The electric field of ten CNTs is stronger than that of 30 CNTs, as shown in Figs. 5 and 6. Because high density of CNTs will have the large screening effect among adjacent emitters and reduce the strength of electric field, the emitted electrons attracted by anode will be fewer.

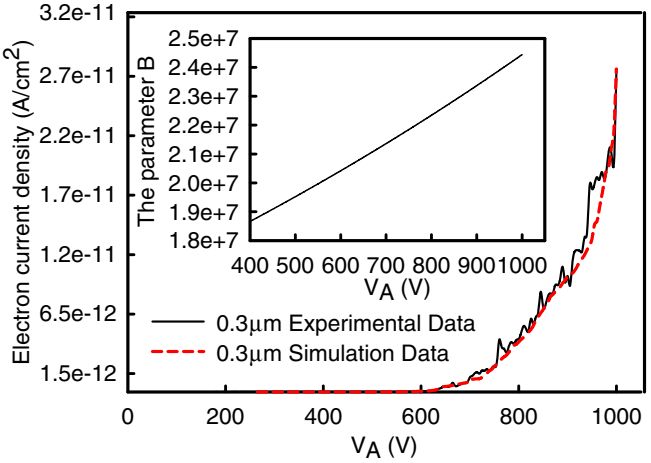

Fig. 3. (Color online) Comparison between the simulation and measurement of the collected emission current for the fabricated AAO–CNTs' triode. The structure is with 30 CNTs with $H = 0.3\,\mu m$ (estimated). The inset is the calibrated parameter B vs the different applied voltage.

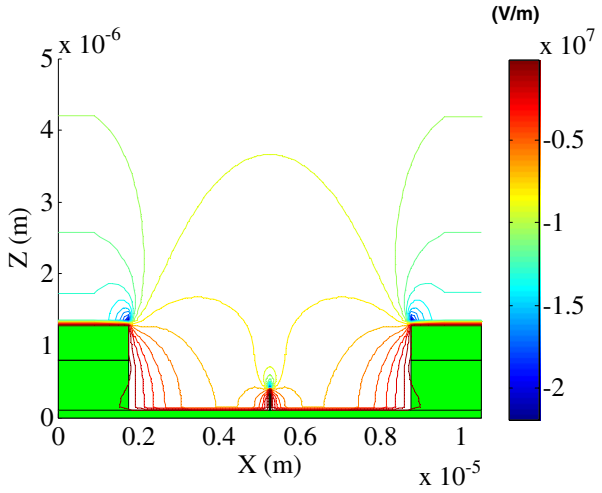

Fig. 4. (Color online) The electric field of the structure with single CNT, where $H = 0.42\,\mu m$, $V_A = 1000\,V$, and $V_G = 0\,V$.

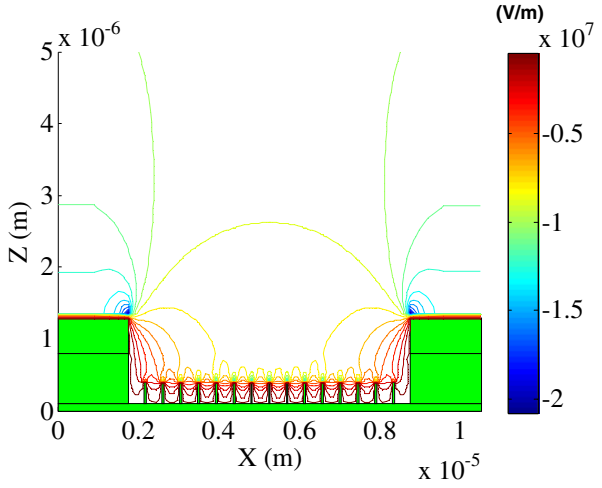

Fig. 5. (Color online) The electric field of the structure with ten CNTs, where the setting is the same with Fig. 4. The electric field is redistributed due to the screening effect.

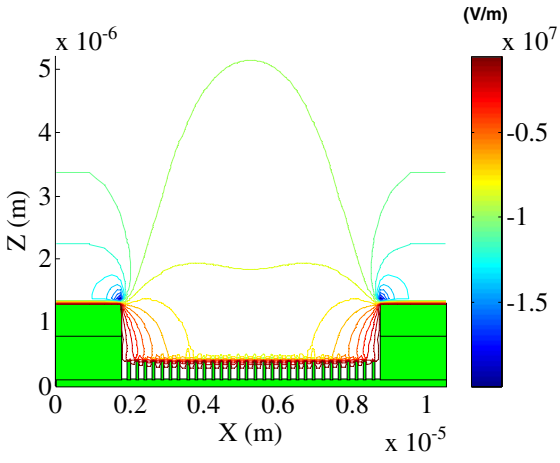

Fig. 6. (Color online) The electric field for the structure with 30 CNTs, where the setting is the same with Fig. 4. The strength of electric field is significantly reduced when the number of CNTs is increased among Figs. 4–6.

Table I. The strength of electric field and collected emission current density for the structure with various numbers of CNTs, where the setting is the same with Fig. 4. The F–N current depends upon the strength of electric field. More than three-order magnitude difference is observed when the number of CNTs is increased from 10 to 30, where $V_A = 1000\,V$, $V_G = 0\,V$.

	Number of CNTs				
	1	10	15	20	30
Spacing between CNTs (μm)	0	0.7	0.467	0.35	0.233
E ($\times 10^6$ V/m)	11.597	11.107	9.067	8.795	5.987
I ($\times 10\,nA/cm^2$)	64.31	63.68	6.751	1.165	0.0642

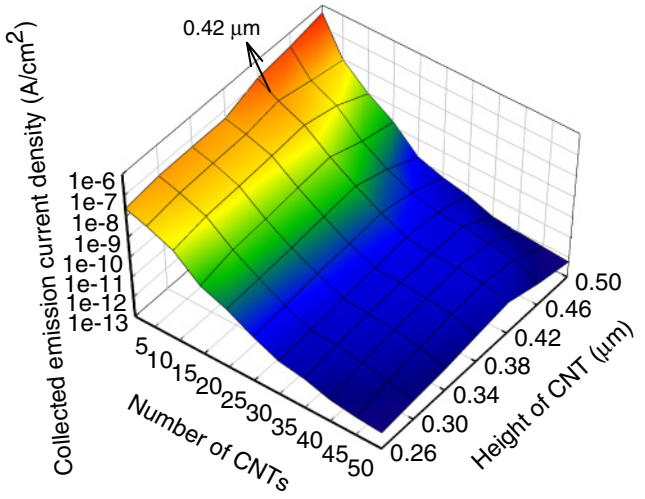

Fig. 7. (Color online) The current density versus the number and height of CNTs, where $V_A = 1000\,V$ and $V_G = 0\,V$.

The theoretically estimated emission currents versus the number of CNTs are summarized in Table I, where the extracted electric fields are included. When the spacing between CNTs decreases from 0.7 to 0.233 μm, the collected emission current density decreases from 637 to 0.64 nA/cm^2. We notice that the significant suppression of the current density depends upon the strength of electric field nonlinearly which is resulting from the screening effect of the explored structure with different spacing of CNTs. The optimal FE property is examined by varying the number and the height (H) of CNTs, as shown in Fig. 7. The theoretically computed collected emission current decreases when the number of CNTs increases for a fixed height. Similarly, for a fixed thickness of oxide (SiO_2) and the number of CNTs, there is an optimal current versus the height of CNTs. Although the structure with a single AAO–CNT may produce the largest collected current than others according the theoretical results shown in Fig. 7, it is difficult to precisely grow only one AAO–CNT with the exact height in the middle of triode structure. We notice that the collected current is at the same level for the structure with less than ten AAO–CNTs. Therefore, according to our simulation cases, as shown in Fig. 7, an optimal condition on the explored structure of AAO–CNTs with the number $= 10$ and $H = 0.42\,\mu m$ could be suggested for obtaining better emission current density among others.

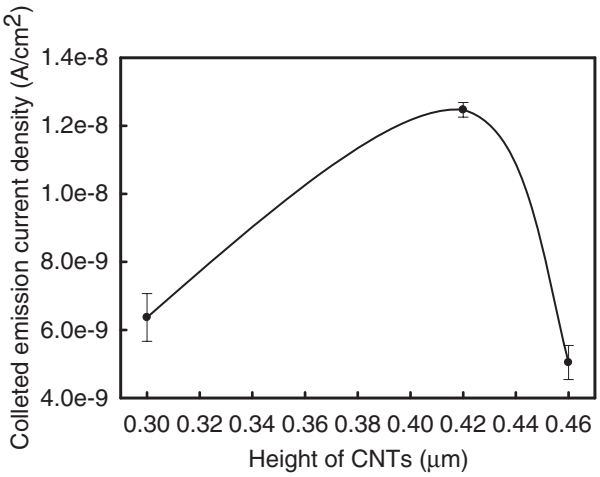

Fig. 8. The fluctuation of current density for 100 random heights, where $3\sigma = 10\%$ height of CNTs, the number of CNTs is 10, $V_A = 1000\,V$, and $V_G = 0\,V$.

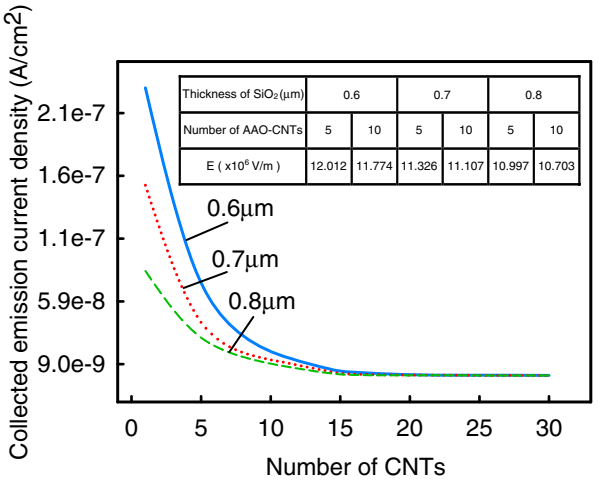

Fig. 9. (Color online) The current density with respect to the thickness of SiO_2 varying from 0.6 to 0.8 μm, where $H = 0.42\,\mu m$, $V_A = 1000\,V$, and $V_G = 0\,V$ are fixed. When the thickness of $SiO_2 = 0.6\,\mu m$, the structure's current attains it maximum for the small number of CNTs due to the suppression of the gate controllability.

The optimal condition is a compromise between the manufacturability of AAO–CNTs and the magnitude of the collected current. A thousandfold difference in the collected current is observed for the structure with 10 and 30 CNTs. The FE efficiency significantly depends upon the variation on the number and height of CNTs. For this optimal setting, we estimate the fluctuation of FE property by randomly generated heights, as shown in Fig. 8. Taking $H = 0.3$, 0.42, and 0.46 μm as the nominal cases, the currents are calculated for the statistically generated 100 heights (where $3\sigma = 10\%$ variation of H is assumed) for all CNTs. The variance (the bars) of the emission current density is small for the case of $H = 0.42\,\mu m$, which implies that the setting has stable FE property. For the obtained $H = 0.42\,\mu m$, the effect of thickness of SiO_2 on the collected current is explored for the structure under $V_A = 1000\,V$ and $V_G = 0\,V$, as shown in Fig. 9. Thicker oxide exhibits lower current because the strength of electric

field, shown in the inset table of Fig. 9, is reduced and also the trajectory of emitted electrons is disturbed. Though the structure with the thinner thickness of SiO_2 has higher current, the triode with a significant reduction of the thickness of SiO_2 will weaken its gate controllability and behave a diode. Therefore, the thickness of SiO_2 also should be taken into consideration when we explore the effect of density and morphology of the CNTs on the uniformity of FE properties of AAO–CNT in the triode structure.

4. Conclusions

In this study, we have explored the FE property of AAO–CNT in the triode structure. According to the calibrated model, emission current of structure has been examined with respect to different density and morphology of the AAO–CNTs. An optimal condition for growth of AAO–CNT triode structure has been found. High density of CNTs will result in large screening effect among adjacent emitters and reduce the strength of electric field. Consequently, it significantly affects the collected emission current density. Significant suppression on the collected emission current density has been predicted when the structure is with high density of CNTs. We are currently planning to fabricate the samples and conduct the corresponding experimental verification. Three-dimensional modeling and simulation is also under performed for studying effect of random position of AAO–CNTs on the FE property of the structure.

Acknowledgments

This work was supported in part by Taiwan National Science Council (NSC) under Contract NSC-96-2221-E-009-210 and Contract NSC-96-2752-E-009-003-PAE, and by the Chunghwa Picture Tubes under a 2006-2008 grant.

1) Y. Huh, J. Y. Lee, J. H. Lee, T. J. Lee, S. C. Lyu, and C. J. Lee: Chem. Phys. Lett. **375** (2003) 388.
2) F. Ito, Y. Tomihari, Y. Okada, K. Konuma, and A. Okamoto: IEEE Electron Device Lett. **22** (2001) 426.
3) J. Li, C. Papadopoulos, J. M. Xu, and M. Moskovits: Appl. Phys. Lett. **75** (1999) 367.
4) P.-L. Chen, C.-T. Kuo, T.-G. Tsai, B.-W. Wu, C.-C. Hsu, and F.-M. Pan: Appl. Phys. Lett. **82** (2003) 2796.
5) C. C. Lin, K. C. Chang, F. M. Pan, C. T. Kuo, M. Liu, and C. N. Mo: Diamond Relat. Mater. **16** (2007) 1388.
6) K. P. Liao, Y. Hu, T. L. Lin, and Y. C. Lan: J. Vac. Sci. Technol. B **25** (2007) 484.
7) C. K. Birdsall and A. B. Langdon: *Plasma Physics via Computer Simulation* (McGraw-Hill, New York, 1985).
8) J. P. Verboncoeur, A. B. Langdon, and N. T. Gladd: Comput. Phys. Commun. **87** (1995) 199.
9) B. Goplen, L. Ludeking, D. Smithe, and G. Warren: Comput. Phys. Commun. **87** (1995) 54.
10) R. H. Fowler and L. W. Nordheim: Proc. R. Soc. London, Ser. A **119** (1928) 173.
11) F. A. Lewis: *The Palladium/Hydrogen System* (Academic Press, London, 1967).
12) M. Lenzlinger and E. H. Snow: J. Appl. Phys. **40** (1969) 278.
13) R. Waters and B. V. Zeghbroeck: Appl. Phys. Lett. **73** (1998) 3692.
14) J. He, P. H. Cutler, and N. M. Miskovsky: Appl. Phys. Lett. **59** (1991) 1644.